Pb-free semiconductor ferroelectrics: A theoretical study of Pd-substituted $Ba(Ti_{1-x}Ce_x)O_3$ solid solutions

Joseph W. Bennett,[1] Ilya Grinberg,[1] Peter K. Davies,[2] and Andrew M. Rappe[1,2]
[1]*The Makineni Theoretical Laboratories, Department of Chemistry, University of Pennsylvania, Philadelphia, Pennsylvania 19104, USA*
[2]*Department of Materials Science and Engineering, University of Pennsylvania, Philadelphia, Pennsylvania 19104, USA*
(Received 16 June 2010; revised manuscript received 29 September 2010; published 10 November 2010)

We use first-principles density-functional-theory calculations to investigate the ground state structures of $Ba(Ti_{1-x}Ce_x)O_3$ solid solutions containing Pd. Previous studies have shown that the properties of $BaTiO_3$, a Pb-free ferroelectric ABO_3 perovskite, can be tailored via *B*-site substitution. In the present study, we substitute Ce for Ti to increase the overall volume of the perovskite, to then accommodate an O-vacancy-stabilized Pd substitution. Using the LDA+*U* method, we predict that these proposed materials will display a decreased band gap compared to $BaTiO_3$ while maintaining polarization. These features, combined with their environmentally friendly characteristics make these materials promising candidates for use as semiconducting ferroelectrics in solar-energy conversion devices.

DOI: 10.1103/PhysRevB.82.184106 PACS number(s): 71.15.Mb, 77.84.−s, 81.05.Zx

I. INTRODUCTION

The need to create stable, single-phase components to be used in photovoltaic devices has recently begun to generate great interest, though candidate materials are few and far between.[1,2] For optimal utilization of the energy in the solar spectrum, a material with a band gap in the range of 1.6–2.0 eV and good charge carrier separation properties to prevent recombination is required. Ferroelectric ABO_3 materials have been shown to exhibit good charge separation properties and have therefore been studied as candidate materials for photovoltaic application, e.g., $BiFeO_3$,[1,3–5] $Pb(Ti_{1-x}M_x)O_{3-\delta}$,[2] and $Pb(Zr_{1-x}Ti_x)O_3$.[6,7]

Substituting the *B*-site of Pb-based perovskites with elements whose bonds with oxygen are less ionic and more covalent has been shown to reduce the band gap.[2] However, solid solutions containing Pb are not environmentally friendly. $BaTiO_3$ is a Pb-free ferroelectric perovskite; many experimental studies have shown that the $BaTiO_3$ band gap can be altered by substituting either the *A* or *B*-site cations, as shown in Fig. 1. In substituting Ba with Sr, the band gap increases with increasing Sr concentration (x=0.1–0.5).[8–12] This same effect is observed when Zn is substituted for Ti (x=0.01–0.05).[13] However, when Co is substituted, the band gap decreases with increasing Co concentration (x=0.01–0.10).[14]

In a previous study, we explored the effects of substituting another transition metal, Pd, into $BaCeO_3$ and found that the presence of Pd stabilized by an O-vacancy decreased the band gap significantly by creating a stable square-pyramidal Pd complex.[15,16] Although $BaCe_{1-x}Pd_xO_3$ is not ferroelectric, solid solutions of $Ba(Ti_{1-x}Ce_x)O_3$ have been synthesized and are reported to demonstrate ferroelectric responses.[17,18] Even though there is a large difference between $r_{Ce^{4+}}$ and $r_{Ti^{4+}}$, 0.87 Å and 0.61 Å respectively, a significant range of single-phase ferroelectric solid solutions can be prepared at high temperature with x values as high as x=0.33.[19] In this study, we substitute the *B*-site of $Ba(Ti_{1-x}Ce_x)O_3$-based solid solutions with Pd, which is stabilized by an accompanying O-vacancy. We predict that the new $Ba(Ti_{1-x}Ce_x)O_3$-derived perovskites display lower band gaps while maintaining most of the polarization of the parent $BaTiO_3$ material.

II. METHODOLOGY

To relax ionic positions and optimize lattice constants, an in-house solid state density-functional-theory (DFT) code, blocked Hamiltonian (BH), employed in previous studies[21,22] is used. The local density approximation (LDA) of the exchange correlation functional and a 4×4×4 Monkhorst-Pack sampling of the Brillouin zone[23] are used for all calculations, except for the response function and Berry phase

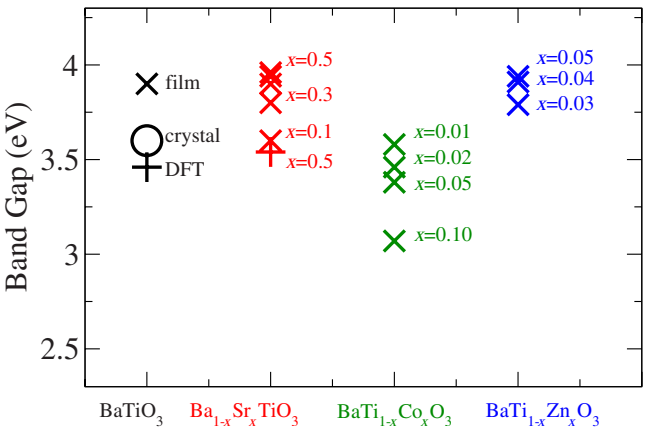

FIG. 1. (Color online) × and open circles denote experimental band gap of thin films and single crystals, respectively. + denotes theoretical band gap of a previous study. For $BaTiO_3$ the band gap of a thin film (Ref. 12) is larger than that of a single crystal (Ref. 20) both of which are slightly larger than those previously predicted by hybrid functional DFT (Ref. 12). In substituting the *A*-site with Sr, the band gap of these films increases with increasing Sr content (Refs. 8–12). Note that hybrid functional DFT also underestimates the E_{gap} for the 1:1 Ba:Sr composition. For *B*-site substitutions, Co doping decreases the band gap with increasing Co content (up to x=0.10) (Ref. 14) while substitution with Zn increases the band gap with increasing Zn content (Ref. 13).

TABLE I. Comparison of experimental (Refs. 17, 40, and 41) and theoretical lattice parameters (Å), polarization along (111) (C/m^2) and LDA+U band gap (eV). Also shown are substituted BT solid solution results from this study, where x_{Ce} is 0.125 and 0.25 for BTC and BTCP is 12.5% Ce and 12.5% Pd. DFT-LDA E_{gap} values are underestimated when compared to experiment, however adding Hubbard U values increases these values to obtain a more accurate trend.

	BT	BT	BTC	BTC	BTCP
	Expt.	Theory	$x_{Ce}=0.125$	$x_{Ce}=0.25$	$x_{Ce}=x_{Pd}=0.125$
a	8.02	8.01	8.26	8.32	7.93
b	8.02	8.01	8.26	8.32	8.05
c	8.02	8.01	8.28	8.32	8.05
P	0.29	0.38	0.34	0.34	0.21
E_{gap}	3.6	3.6	3.5	3.5	1.6

polarization[24] calculations, for which a $6\times6\times6$ grid was required to achieve convergence. We did not use the generalized gradient approximation of the exchange-correlation functional, as it overestimates relaxed volumes, affecting the polarization.[25] All atoms are represented by norm-conserving optimized[26] designed nonlocal[27] pseudopotentials, generated with the OPIUM code.[28] All calculations are performed with a plane wave cutoff of 50 Ry, on a $2\times2\times2$ 40 atom supercell arrangement, except those which included an O vacancy which were performed on a 39 atom supercell arrangement. For each supercell composition, calculations were performed on three to four different supercells, which led to similar results for each set. Structural DFT results for $BaTiO_3$, as shown in Table I, agree well with experimental data.

As expected, DFT-LDA calculations underestimate the band gap of $BaTiO_3$, in line with the well-known trend of DFT underestimation of band gaps.[29–32] Although LDA underestimates the band-gap magnitudes, DFT calculations have been shown to be reliable in reproducing trends in the band gap as the material composition is changed.[33] To correct the band gaps of our supercells, we use the LDA+U method,[34] as employed in the QUANTUM-ESPRESSO software package.[35] To pick the values of the Hubbard U, we adjust U for Ti, Ce, Pd, and O to match the experimental band-gap values for $BaTiO_3$, $BaCeO_3$, and PdO. We find that U values of 8.0 eV, 11.0 eV, 8.0 eV, and 3.0 eV for Ti($3d$), Ce($4f$), Pd($4d$), and O($2p$) respectively, are necessary to reproduce the experimental band-gap data, and we use these values of U for all compositions in our study. Our LDA+U results for the computed band gaps are presented in Fig. 2. See Ref. 36 for a detailed analysis of how the band gap changes as a function of U.[36]

III. RESULTS

Comparison of $Ba(Ti_{1-x}Ce_x)O_3$ solid solutions to $BaTiO_3$ show that the addition of Ce to a $2\times2\times2$ $BaTiO_3$ supercell increases the lattice constant from 8.00 Å to at least 8.26 Å ($x_{Ce}=0.125$). At this concentration of Ce, the supercell is essentially pseudocubic, with a small (0.2%) difference between $a=8.26$ Å and $c=8.28$ Å lattice constants, as shown in Table I. This result is in agreement with previous experimental studies,[17,18] where solid solutions with $x>6\%$ were pseudocubic and only those below that threshold were tetragonal, though it disagrees slightly with the lattice constant trend proposed in Ref. 19. In that study, as x_{Ce} increased, c/a increased to ≈1.01 at $x_{Ce}=0.25$. This deviation is minor, and for the purposes of our paper, we assume pseudocubic symmetry at this x.

For $x_{Ce}=0.25$, in a $2\times2\times2$ supercell, there are three possible ways to arrange the two Ce atoms, along either the (100), (101), or (111) direction. We find that for the supercells examined, the most energetically favorable structure has two Ce oriented along (101). The optimized lattice constants are cubic ($a=8.32$ Å) and are slightly larger than those observed experimentally (8.24 Å). Comparison of the energy differences shows that the (101) orientation is favored over (111) by 0.35 eV and over the (100) orientation by 0.86 eV per 40 atom cell.

The replacement of Ce-O by an O-vacancy-stabilized Pd decreases the lattice constants by about 0.20 Å, even though an elongated apical Pd-O bond is present along (100). This elongation is caused by the strong preference of Pd to form a

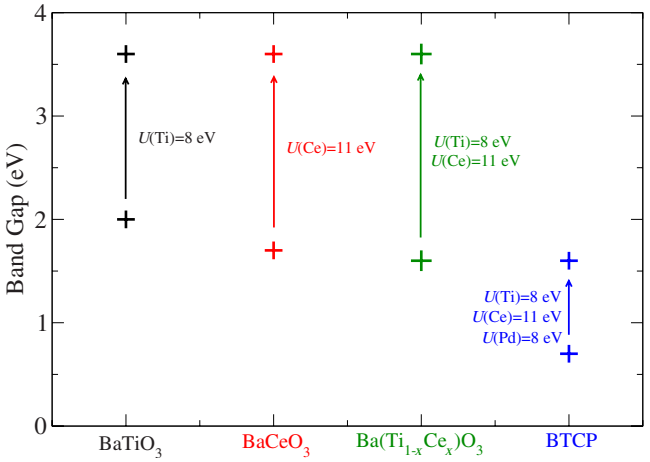

FIG. 2. (Color online) Presented here from left to right are the DFT-LDA (at bottom) band gaps of $BaTiO_3$, $BaCeO_3$, $Ba(Ti_{1-x}Ce_x)O_3$, and BTCP solid oxides respectively. Arrows show the increase in band gap after LDA+U correction (at top). U value for O is 3 eV while values for cations vary, as indicated in the plot.

TABLE II. Average cation displacements D_{avg} in Å for the lowest energy structure of each set of solid solutions of different compositions. The addition of Ce to $BaTiO_3$ in supercells $x_{Ce}=0.125$ and $x_{Ce}=0.25$ increase the lattice constants, causing increased cation displacements. When Pd is substituted for one-half of the Ce as in BTCP, cation displacements increase, though the O vacancy influences Pd and Ce to displace along (100) and not (111). Also reported are the range of $M-O$ bond lengths in Å for comparison.

Structure	Cation	D_{avg}	Axis	$M-O$
BT	Ba	0.08	(111)	2.77–2.89
	Ti	0.22	(111)	1.88, 2.11
$x_{Ce}=0.125$	Ba	0.15	(111)	2.75–3.11
	Ti	0.33	(111)	1.85–2.34
	Ce	0.02	(111)	2.19–2.33
$x_{Ce}=0.25$	Ba	0.14	(111)	2.78–3.11
	Ti	0.34	(111)	1.81–2.34
	Ce	0.02	(111)	2.21–2.27
BTCP	Ba	0.27	(111)	2.73–3.06
	Ti	0.28	(111)	1.85–2.33
	Ce	0.14	(100)	2.03, 2.19
	Pd	0.18	(100)	2.06, 2.37

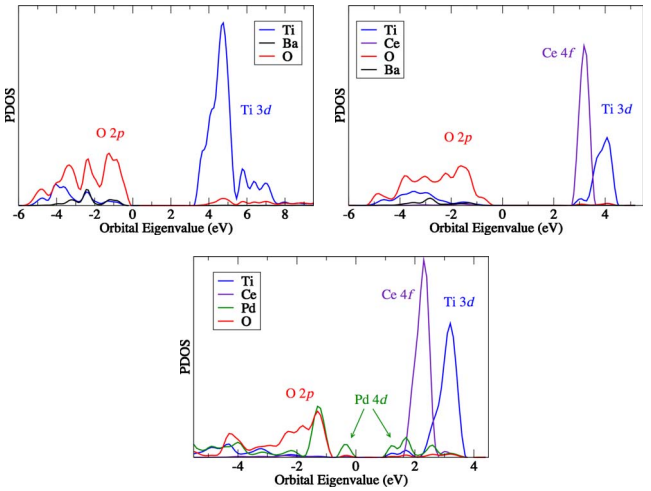

FIG. 3. (Color online) Projected density of states analysis shows that the electronic structure of (a) $BaTiO_3$ differs greatly from (b) $Ba(Ti_{0.875}Ce_{0.125}O_3)$, and (c) $Ba(Ti_{0.75}Ce_{0.125}Pd_{0.125})O_{3-\delta}$. While Ba (black) does not contribute to the states surrounding E_{gap}, combinations of Ti $3d$ (blue), Pd $4d$ (green), Ce $4f$ (magenta), and O $2p$ (red) states compose the various HOMOs and LUMOs. Values are similar for (a) and (b) but decrease markedly for (c) with the introduction of an O-vacancy stabilized Pd.

square planar complex with its equatorial O so the remaining apical O is forced 0.3 Å away from Pd.

Examination of the energy differences of the three possible arrangements of the Ce atom relative to the O vacancy stabilized Pd shows that the lowest energy arrangement is for the Ce and Pd atoms to be placed along the (100) direction with the O vacancy in between. This preference is quite strong as the energy of the next lowest B-cation arrangement, placement of Ce along (111) relative to Pd-O vacancy along (100), is more than 1 eV higher in total energy. This indicates that fivefold coordinate Ti atoms are much less stable than the fivefold coordinated Ce atoms.

The displacements and polarization of the material are strongly affected by changes in the Ce and Pd content. The substitution of 12.5% Ce in $Ba(Ti_{1-x}Ce_x)O_3$ causes Ba to displace twice as far as in $BaTiO_3$, as shown in Table II. The Ti displacements increase from 0.22 Å in $BaTiO_3$ to 0.33 Å in $Ba(Ti_{0.875}Ce_{0.125})O_3$, due to the increased overall volume of the supercell. However, the Ce dopants do not displace (Table II), mostly likely because of their large size. This magnitude of average displacements changes little as the fraction of Ce is doubled to $x=25\%$. The displacement magnitudes of the Ti cations show some degree of variation that depends on their proximity to the Ce atoms. Ti atoms which are the closest to Ce displace the least (0.3 Å) while those farther away displace more (0.4 Å).

The changes in displacements discussed above give rise to changes in the overall polarization of the material. Our calculations show that $Ba(Ti_{0.875}Ce_{0.125})O_3$ has $P=0.34$ C/m^2, slightly lower than in BT ($P=0.38$ C/m^2). Using the proportionality of the transition temperature to the square of polarization established previously[37–39] and the well-known value for the Curie temperature of $BaTiO_3$ (410 K), we can predict a transition temperature of 330 K for $Ba(Ti_{0.875}Ce_{0.125})O_3$, in excellent agreement with the 320 K observed experimentally. When another Ce is added to the supercell ($x=0.25$), the total volume increases further, though Ce still does not displace as readily as Ti. We find polarization magnitudes of 0.34 C/m^2 [Ce-Ce along (101)], 0.38 C/m^2 [Ce-Ce along (101)], and 0.25 C/m^2 [Ce-Ce along (100)] for the three $x=0.25$ supercells studied (from lowest to highest energy).

Using the lowest energy structure, where Ce are oriented along (101), we obtain a $P=0.34$ C/m^2 at 0 K, corresponding to a T_c of 330 K. This is only in qualitative agreement with experimental results, where T_c of the $x=0.25$ composition is extrapolated to be 210 K. We believe that at $x=0.25$, very close to the experimental solubility limit due to Ce clustering the structure may resemble a solid solution whose composition is closer to $\frac{1}{2}BaTiO_3-\frac{1}{2}Ba(Ti_{0.5}Ce_{0.5})O_3$. Therefore, the (111) and (101) ordered supercells which do not represent Ce clustering well, overestimate the polarization magnitude of the material. The (100) ordered supercell, which most closely resembles Ce clustering and in $\frac{1}{2}BaTiO_3-\frac{1}{2}Ba(Ti_{0.5}Ce_{0.5})O_3$, exhibits P of 0.25 C/m^2, corresponding to $T_c=180$ K, in much closer agreement to the experimental trend.

When an O-vacancy-stabilized Pd is substituted for Ce to create $Ba(Ti_{0.75}Ce_{0.125}Pd_{0.125})O_{3-\delta}$ (BTCP), the solid solution shows an increased displacement along (111) for both Ba and Ti when compared to the parent $BaTiO_3$ material, though the Ti displacements are decreased when compared to $Ba(Ti_{1-x}Ce_x)O_3$ solid solutions. The Ba atoms closest to the vacancy displace 0.50 Å along (111) while those furthest displace only 0.10 Å. The increased off-centering of Ba is most likely caused by the effects of the O-vacancy along (100). The B-sites closest to the O-vacancy, Pd and Ce, displace in (100) toward the vacancy (from opposite sides) as

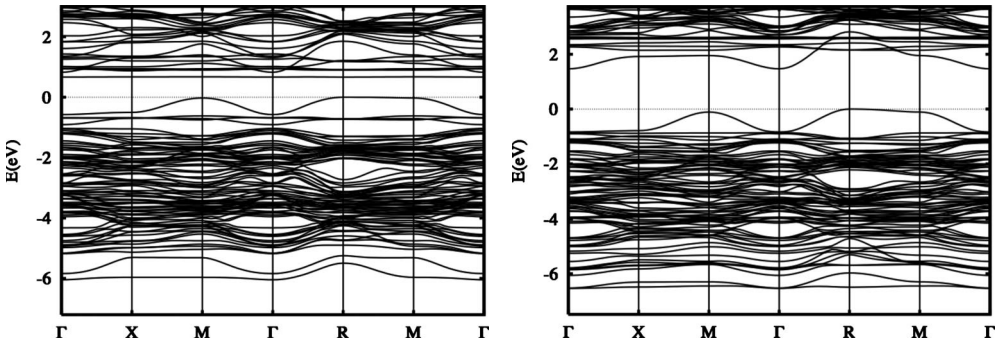

FIG. 4. Electronic band structure of BTCP solid solution from (a) DFT-LDA calculations and (b) LDA+U calculations. In applying Hubbard U values of 8.0, 11.0, 8.0 and 3.0 eV to Pd(4d), Ce(4f), Ti(3d), and O(2p), the band gap increases from 0.6 eV (R to R) to 1.6 eV (R to Γ).

the remaining apical O of Pd is forced away to create a square planar environment around Pd. The interruption caused by the vacancy forces Ba to displace further than it normally would, as it attempts to avoid creating a stronger Ba-O bond along (100). Since the Born effective charges of the B-site ions are much greater than those of the Ba atoms, the effects of the increased Ba displacements are more than counterbalanced by the decreased B-site displacements, resulting in a decreased P of 0.21 $\mathrm{C/m^2}$ for BTCP.

In the solid solution $Ba(Ti_{0.75}Ce_{0.125}Pd_{0.125})O_{3-\delta}$, the substitution of Pd for Ce decreases E_{gap} for all Ce/Pd arrangements. The orientation of Pd in the preferred square planar arrangement introduces new states in both the highest occupied molecular orbital (HOMO) and the lowest unoccupied molecular orbital (LUMO) that are mainly d-orbitals. As shown in Fig. 3(a), in $BaTiO_3$ the HOMO is localized around O, its 2p orbitals interacting slightly with the 3d-orbitals of Ti. The LUMO is localized around Ti and resembles 3d states. The addition of Ce, to form the solid solution $Ba(Ti_{0.875}Ce_{0.125}O_3)$, decreases the band gap from 3.6 to 3.5 eV [Fig. 3(b)], as Ce 4f states become the LUMO. When the Pd and O vacancy are added, Pd d-states fall in the $BaTiO_3$ band gap, reducing the band gap of the alloy [Fig. 3(c)]. The HOMO is localized around Pd, and is mainly d_{z^2}, the highest filled d-orbital for a d^8 metal in a square-planar configuration. The LUMO is also localized around Pd, resembling $d_{x^2-y^2}$. This Pd d-state is lower in energy than the Ti 3d, lowering the conduction band edge relative to either $BaTiO_3$ or $Ba(Ti_{1-x}Ce_x)O_3$ solid solution.

The DFT-LDA calculated band gap of BTCP solid solution is 0.6 eV, which corresponds to a direct transition from R to R, as shown in Fig. 4(a). When Hubbard U values are applied, this value, as well as the nature of the transition, change [Fig. 4(b)] ; the band gap increases as the transition goes from direct to indirect. However, even the LDA+U band gap is still smaller than that of either $BaTiO_3$ or $BaCeO_3$, as shown in Fig. 2.

With the decreased band gap, all Pd-substituted solid solutions are now better suited to absorb visible light than $BaTiO_3$, however this substitution does decrease P. For $BaTiO_3$, our DFT calculated $P=0.38$ $\mathrm{C/m^2}$ ($\vec{P}_x=\vec{P}_y=\vec{P}_z=0.22$ $\mathrm{C/m^2}$) is higher than that of $Ba(Ti_{0.75}Ce_{0.125}Pd_{0.125})O_{3-\delta}$, where $P=0.20$ $\mathrm{C/m^2}$. This decrease is attributed to $\vec{P}_x<0.1$, as both Ce and Pd displace along (100) toward the O vacancy from either side and not along (111), the direction of the concerted motion of the other cations. Though the polarization is decreased, the material remains polar, displays a decreased band gap and is Pb-free. The scheme presented here could potentially increase the solar efficiency of the next generation of solid oxide components in solar photovoltaics and hydrogen production devices.[42]

IV. CONCLUSION

We have presented the ground-state structures of Pd-substituted $Ba(Ti_{1-x}Ce_x)O_3$, new Pb-free solid state oxide alloys that decrease the band gap while maintaining spontaneous polarization. These materials could be used in solar hydrogen production and photovoltaic applications because they can both absorb sunlight and separate carriers via the anomalous bulk photovoltaic effect seen in polarized materials.[43] These combined properties could make these new materials more efficient at first trapping and then utilizing more of the solar spectrum than previous components of solar conversion devices.

ACKNOWLEDGMENTS

J.W.B. and A.M.R. were supported by the Department of Energy Office of Basic Energy Sciences, under Grant No. DE-FG02-07ER46431. I.G. was supported by the Office of Naval Research, under Grant No. N00014-09-1-0157 and P.K.D. under Grant No. N00014-09-1-0455. Computational support was provided by U.S. DoD, by a DURIP grant, and by a Challenge Grant from the HPCMO.

[1] T. Choi, S. Lee, Y. Choi, V. Kiryukhin, and S.-W. Cheong, Science **324**, 63 (2009).
[2] J. W. Bennett, I. Grinberg, and A. M. Rappe, J. Am. Chem. Soc. **130**, 17409 (2008).
[3] S. R. Basu, L. W. Martin, Y. H. Chu, M. Gajek, R. Ramesh, R. C. Rai, X. Xu, and J. L. Musfeldt, Appl. Phys. Lett. **92**, 091905 (2008).
[4] A. J. Hauser, J. Zhang, L. Mier, R. A. Ricciardo, P. M. Woodward, T. L. Gustafson, L. J. Brillson, and F. Y. Yang, Appl. Phys. Lett. **92**, 222901 (2008).
[5] S. Y. Yang *et al.*, Appl. Phys. Lett. **95**, 062909 (2009).
[6] V. K. Yarmarkin, B. M. Gol'tsman, M. M. Kazanin, and V. V. Lemanov, Phys. Solid State **42**, 522 (2000).
[7] K. K. Uprety, L. E. Ocola, and O. Auciello, J. Appl. Phys. **102**, 084107 (2007).
[8] G. S. Wang, J. Yu, Q. Wang, Q. Zhao, J. L. Sun, X. J. Meng, S. L. Guo, and J. H. Chu, Phys. Status Solidi A **194**, 56 (2002).
[9] H. Tian, W. Luo, X. Pu, P. Qiu, X. He, and A. Ding, Solid State Commun. **117**, 315 (2001).
[10] S. B. Singh, H. B. Sharma, H. N. K. Sarma, and S. Phanjoubam, Physica B **403**, 2678 (2008).
[11] P. K. Sharma, G. L. Messing, and D. K. Agrawal, Thin Solid Films **491**, 204 (2005).
[12] S. Dorfman, S. Piskunov, E. A. Kotomin, and D. Fuks, Phys. Scr. **T118**, 276 (2005).
[13] A. Fasasi, M. Maaza, E. Rohwer, D. Knoessen, C. Theron, A. Leitch, and U. Buttner, Thin Solid Films **516**, 6226 (2008).
[14] Y. W. Li, J. L. Sun, X. J. Meng, J. H. Chu, and W. F. Zhang, Appl. Phys. Lett. **85**, 1964 (2004).
[15] J. Li, U. G. Singh, J. W. Bennett, K. Page, J. C. Weaver, J.-P. Zhang, T. Proffen, A. M. Rappe, S. Scott, and R. Seshadri, Chem. Mater. **19**, 1418 (2007).
[16] U. G. Singh, J. Li, J. W. Bennett, A. M. Rappe, R. Seshadri, and S. L. Scott, J. Catal. **249**, 349 (2007).
[17] C. Ang, Z. Yu, Z. Jing, R. Guo, A. S. Bhalla, and L. E. Cross, Appl. Phys. Lett. **80**, 3424 (2002).
[18] Z. Jing, Z. Yu, and C. Ang, J. Mater. Sci. **38**, 1057 (2003).
[19] A. Chen, Y. Zhi, J. Zhi, P. M. Vilarinho, and J. L. Baptista, J. Eur. Chem. Soc. **17**, 1217 (1997).
[20] M. N. Kamalasanan, S. Chandra, P. C. Joshi, and A. Mansingh, Appl. Phys. Lett. **59**, 3547 (1991).
[21] J. W. Bennett, I. Grinberg, and A. M. Rappe, Phys. Rev. B **73**, 180102(R) (2006).
[22] J. W. Bennett, I. Grinberg, and A. M. Rappe, Chem. Mater. **20**, 5134 (2008).
[23] H. J. Monkhorst and J. D. Pack, Phys. Rev. B **13**, 5188 (1976).
[24] R. Resta, Rev. Mod. Phys. **66**, 899 (1994).
[25] Z. Wu, R. E. Cohen, and D. J. Singh, Phys. Rev. B **70**, 104112 (2004).
[26] A. M. Rappe, K. M. Rabe, E. Kaxiras, and J. D. Joannopoulos, Phys. Rev. B **41**, 1227 (1990).
[27] N. J. Ramer and A. M. Rappe, Phys. Rev. B **59**, 12471 (1999).
[28] http://opium.sourceforge.net
[29] L. J. Sham and M. Schlüter, Phys. Rev. Lett. **51**, 1888 (1983).
[30] L. J. Sham and M. Schlüter, Phys. Rev. B **32**, 3883 (1985).
[31] M. S. Hybertsen and S. G. Louie, Phys. Rev. Lett. **55**, 1418 (1985).
[32] M. S. Hybertsen and S. G. Louie, Phys. Rev. B **34**, 5390 (1986).
[33] C. G. Van de Walle and R. M. Martin, Phys. Rev. B **34**, 5621 (1986).
[34] V. I. Anisimov, J. Zaanen, and O. K. Andersen, Phys. Rev. B **44**, 943 (1991).
[35] P. Giannozzi *et al.*, J. Phys.: Condens. Matter **21**, 395502 (2009).
[36] See supplementary material at http://link.aps.org/supplemental/10.1103/PhysRevB.82.184106 for a detailed analysis of how E_{gap} changes as a function of U.
[37] S. C. Abrahams, S. K. Kurtz, and P. B. Jamieson, Phys. Rev. **172**, 551 (1968).
[38] I. Grinberg and A. M. Rappe, Phys. Rev. B **70**, 220101 (2004).
[39] I. Grinberg and A. M. Rappe, Phys. Rev. Lett. **98**, 037603 (2007).
[40] S. Tinte, M. G. Stachiotti, S. R. Phillpot, M. Sepliarsky, D. Wolf, and R. L. Migoni, J. Phys.: Condens. Matter **16**, 3495 (2004).
[41] P. C. Joshi and S. B. Desu, Thin Solid Films **300**, 289 (1997).
[42] Y. Inoue, K. Sato, K. Sato, and H. Miyama, J. Phys. Chem. **90**, 2809 (1986).
[43] V. M. Fridkin, Crystallogr. Rep. **46**, 654 (2001).